PROCEEDINGS, 45th Workshop on Geothermal Reservoir Engineering
Stanford University, Stanford, California, February 10-12, 2020
SGP-TR-216

Simulations of the 3D Geothermal Heat Flow in Fractured Media

Elchin E. Jafarov[1], Nataliia Makedonska[1], Satish Karra[1], Rajesh Pawar[1], Joe Beisman[1], Ghanashyam Neupane[2], Paul C. Schwering[3], Timothy J. Kneafsey[4], and EGS Collab Team[*]

1. Earth and Environmental Sciences Division, Los Alamos National Laboratory, Los Alamos, New Mexico, USA

2. Idaho National Laboratory, Idaho Falls, Idaho, USA

3. Sandia National Laboratories, Albuquerque, New Mexico, USA

4. Lawrence Berkeley National Laboratory, Berkeley, California, USA

elchin@lanl.gov

Keywords: modeling, hydrothermal simulations, dfnWorks, PFLOTRAN, EGSCollab

ABSTRACT

Understanding heat exchange from injected fluid in subsurface fractured media is crucial for successful operation of enhanced geothermal systems (EGS). To complement our understanding of the EGS-Collab Experiment 1 site, we performed geothermal numerical simulations by modeling heat flow and tracer transport through three-dimensional fractured media. Different conceptual models of fracture geometry setups were used for the heat-flow-transport numerical simulations. Prior to flow simulations: (i) we mapped fractures geometry into continuum computational mesh; (ii) rescaled aperture and permeability of fractures and rock matrix; (iii) projected injection, production and monitoring wells into the simulation domain according to their known locations.

To account for coupled matrix and fracture heat-flow-transport, we employed novel modeling approach by translating the fracture systems to subsurface flow and reactive transport model. We used dfnWorks software to generate fracture networks and PFLOTRAN to simulate heat-flow-transport dynamics. The cold liquid water injection was simulated by using temperatures time-series at the injection source according to hourly averaged temperature data used at injection well at the Experiment 1 site. In addition, we included temperature gradient between injection and production wells to illustrate its effect on simulated temperatures at the producing wells. Our simulations showed that tracer behavior depends on fracture geometry setup. Thermal simulations using three different fracture configurations showed that faster heat response between injection and production wells can be achieved when there is a direct channel linking these two wells.

1. INTRODUCTION

The Enhanced Geothermal System Collaboration (EGS Collab) project is a multi-institution effort, sponsored by the US Department of Energy's Geothermal Technologies Office, with the overarching goal of validating physical/chemical models of hydraulically-stimulated crystalline rock (Kneafsey et al., 2018). The EGS Collab project is tasked with establishing mesoscale (10's of m) field test beds for stimulation and inter-well flow tests that provide a basis for understanding the fracture stimulation methods, resulting fracture geometries, and processes that control heat transfer between rock and stimulated fractures. This project was designed to complement and inform the Frontier Observatory for Research in Geothermal Energy (FORGE) project by testing tools, codes, and concepts that could be scaled-up and employed at FORGE. EGS Collab thus serves as an important research and development step between laboratory-scale stimulation and rock mechanics studies and full-scale FORGE investigations (U.S. Department of Energy, 2017).

Following evaluation of information from several sites, the EGS Collab team selected the 4850 Level of the Sanford Underground Research Facility (SURF) in South Dakota as the site for Experiment 1 (Dobson et al., 2017). EGS Collab Experiment 1 (Expt 1) was

[*] J. Ajo-Franklin, T. Baumgartner, K. Beckers, D. Blankenship, A. Bonneville, L. Boyd, S. Brown, J.A. Burghardt, C. Chai, Y. Chen, B. Chi, K. Condon, P.J. Cook, D. Crandall, P.F. Dobson, T. Doe, C.A. Doughty, D. Elsworth, J. Feldman, Z. Feng, A. Foris, L.P. Frash, Z. Frone, P. Fu, K. Gao, A. Ghassemi, Y. Guglielmi, B. Haimson, A. Hawkins, J. Heise, C. Hopp, M. Horn, R.N. Horne, J. Horner, M. Hu, H. Huang, L. Huang, K.J. Im, M. Ingraham, E. Jafarov, R.S. Jayne, S.E. Johnson, T.C. Johnson, B. Johnston, K. Kim, D.K. King, T. Kneafsey, H. Knox, J. Knox, D. Kumar, M. Lee, K. Li, Z. Li, M. Maceira, P. Mackey, N. Makedonska, E. Mattson, M.W. McClure, J. McLennan, C. Medler, R.J. Mellors, E. Metcalfe, J. Moore, C.E. Morency, J.P. Morris, T. Myers, S. Nakagawa, G. Neupane, G. Newman, A. Nieto, C.M. Oldenburg, T. Paronish, R. Pawar, P. Petrov, B. Pietzyk, R. Podgorney, Y. Polsky, J. Pope, S. Porse, J.C. Primo, C. Reimers, B.Q. Roberts, M. Robertson, W. Roggenthen, J. Rutqvist, D. Rynders, M. Schoenball, P. Schwering, V. Sesetty, C.S. Sherman, A. Singh, M.M. Smith, H. Sone, E.L. Sonnenthal, F.A. Soom, P. Sprinkle, C.E. Strickland, J. Su, D. Templeton, J.N. Thomle, V.R. Tribaldos, C. Ulrich, N. Uzunlar, A. Vachaparampil, C.A. Valladao, W. Vandermeer, G. Vandine, D. Vardiman, V.R. Vermeul, J.L. Wagoner, H.F. Wang, J. Weers, N. Welch, J. White, M.D. White, P. Winterfeld, T. Wood, S. Workman, H. Wu, Y.S. Wu, E.C. Yildirim, Y. Zhang, Y.Q. Zhang, Q. Zhou, M.D. Zoback

designed to focus on hydrofracturing processes. Preliminary numerical studies were done to address borehole notching, thermal environment surrounding the drift, and hydraulic fracturing under a stress gradient (White et al., 2017). The post-experimental numerical simulations are necessary for hypothesis testing and obtaining new insights about collected data.

The main objective of this study is to apply the dfnWorks–PFLOTRAN modeling framework to better understand flow dynamics, heat exchange, and chemical transport in the Expt 1 site. Here we employ, coupled dfnWorks and PFLOTRAN numerical models to simulate full 3D hydrothermal flow and chemical transport, where different fracture setups were considered. dfnWorks (Hyman et al., 2015) is a parallelized computational suite based on Discrete Fracture Network (DFN) model (Dershowitz, 1984). DFN model was chosen due to its ability to represent individual fractures as two-dimensional planar objects, and to place them in a three-dimensional domain, where fractures intersect each other and form fracture networks. We used this capability to model Common DFN (Roggenthen and Doe, 2018, Schwering et al., 2018), where fracture locations and orientations were defined from boreholes core inspections at the experimental site. Makedonska et al., (2020) documented a dfnWorks workflow developed for flow paths simulations at EGS Collab site, where flow travels along Common DFN surrounded by stochastic fracture networks. In the current work we used a new approach to map triangular mesh of fracture network into continuum volume grid, which is used by PFLOTRAN to perform heat-flow simulations. PFLOTRAN is subsurface flow and reactive transport model that solves a system of nonlinear partial differential equations describing multiphase, multicomponent, and multiscale reactive flow and transport in porous media (Hammond et al., 2014). Applications of the PFLOTRAN include energy, climate and nuclear waste disposal (Makedonska et al, 2015), CO_2 sequestration (Lichtner and Karra, 2014; Lu and Lichtner, 2007), enhanced geothermal systems (Lichtner and Karra, 2014; Mudunuru et al., 2017), groundwater contamination (Hammond and Lichtner 2010), hydraulic fracturing (Middleton et al, 2015; Karra et al., 2015), and Arctic hydrology and climate (Karra et al., 2014). The primary rationale for using this dfnWorks–PFLOTRAN framework in our study is an ability for massive high-performance parallelization and state-of-art of the chosen modeling tools.

2. METHOD

In this section we describe the methodology that we used to model heat flow and tracer transport. First, we provide a summary of the Expt 1 site design, then we describe how we scaled up finer scale geometry to a coarser continuum mesh, followed by testing three different fracture networks, and finalizing with the setup of flow and tracer modeling experiments.

2.1 Summary of the Expt 1 site

Description of the Expt 1 (E1) site geology and borehole setup are well-documented by Kneafsey et al. (2018), White et al. (2019), and Neupane et al. (2019). Here we provide a short overview required for understanding our modeling set up. Eight boreholes were drilled from the drift: 1) injection [E1-I], 2) production [E1-P], 3) two fracture-orthogonal monitoring [E1-OT, E1-OB], 4) two deep fracture-parallel monitoring [E1-PDT, E1-PDB], and 5) two shallow fracture-parallel monitoring [E1-PST, E1-PSB]. All boreholes were drilled sub-horizontally from the drift. The map-view schematic representation of the drilled boreholes is shown in Figure 1.

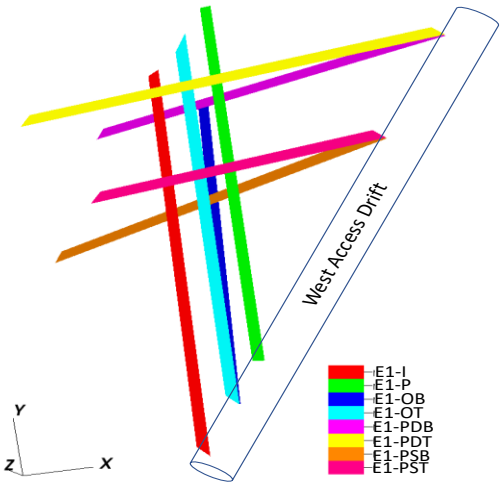

Figure 1: Straight colored lines represent borehole layout within the Expt-1 testbed. Injection [E1-I] borehole shown in red and production [E1-P] borehole shown in green, other six boreholes are the monitoring wells. Y axis indicates north, X is east.

2.2 Mapping a discrete fracture network into a continuum mesh

Natural and hydraulic fractures conduct the main flow at subsurface energy reservoirs and provide the fast path for injected flow. In our model, fractures are generated using dfnWorks tool. However, using dfnWorks, simulations of flow and transport take place in fractures only and no rock matrix is considered, and thus, heat diffusion in the matrix cannot be modeled using a two-dimensional DFN mesh. We describe our approach on mapping DFN triangular mesh into 3D continuum uniform mesh on the example of Common DFN (CDFN) observed at Expt 1 site (Roggenthen and Doe, 2018, Schwering et al., 2018). Location and orientation of individual fractures are defined from core and wireline logs and mapped into FracMan software, Golder Associates Inc., (Dershowitz, 2014), by the members of the EGS

Collab DFN team (Roggenthen and Doe, 2018, Schwering et al., 2018, Ulrich et al, 2018). The first step was to reproduce the fractures generated in FracMan (Figure 2a) into dfnWorks software, keeping their location and orientation the same as they are defined in (CDFN) (Figure 2b). The second step was to generate continuum volume mesh containing fractures that could be passed to the PFLOTRAN model.

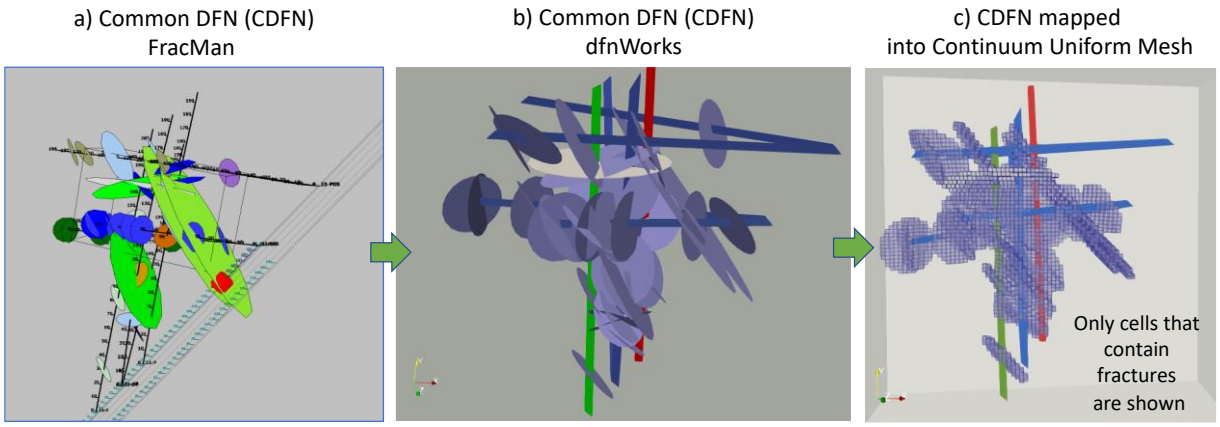

Figure 2: Mapping of fractures geometry into continuum volume mesh: the fracture locations and orientations defined for CDFN in FracMan (a) are reproduced at dfnWorks (b) and mapped into continuum volume mesh (c). The continuum mesh shows only containing fracture grid cells. Here, E1-I is colored in green and E1-P is colored in red.

The meshing toolbox LaGriT (LaGriT, 2013) was used to map discrete fractures (Figure 2b) into continuum mesh (Figure 2c). We defined the size of volume cells and the number of computational cells to generate a continuum mesh. The length and width of the simulation domain was equal to 260 ft (72.9 m), and the height was equal to 140 ft (42.7 m); the total volume of the domain was 260 x 260 x 140 ft^3. The grid cell resolution in the continuum mesh was equal to 1.0 ft^3. The total number of volume cells in the mesh was equal to 9,464,000. The position of each voxel within the continuum mesh (i.e. a value on a regular grid in three-dimensional space) was matched to the fracture's triangular positions. The final continuum mesh had only two cell types: the volume cell that contain fracture (Figure 2c); and the volume cell that belong to rock matrix. If a fracture crosses a voxel, then we assigned that voxel to the corresponding cell type.

We used the rescaling approach to assign porosity and hydraulic permeability to each type of volume cells. The voxels within the continuum mesh not containing fractures were assigned to matrix rock porosity and hydraulic permeability.

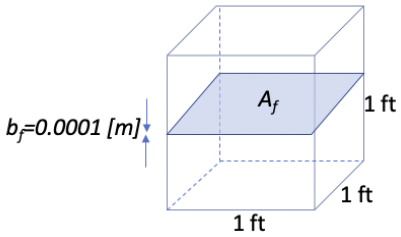

Figure 3: The volume mesh of the size 1.0 ft^3 contains fracture with 0.1mm aperture, b_f=0.1 mm; A_f is the fracture area in the volume cell.

Figure 3 shows an example of a volume cell that contains a fracture portion. To calculate porosity for volume cells that contain fracture we used the following formulation:

$$\phi = V_f / V_c, \tag{1}$$

where V_f is the fracture volume inside a cell and V_c is the volume of the cell that intersects the fracture (V_c=1.0 ft^3). The fracture volume at the cell is equal to the planar fracture area within the cell multiplied by the fracture aperture, b_f. In our simulations all fractures are assigned to the same uniform aperture, 0.1 mm.

To rescale fracture permeability for volume cell, we used Darcy's model assuming that the flow rate is uniform along the cross-section area of the cell. This led us to the following equation:

$$k_c = k_f A_f / A_c. \tag{2}$$

Here k_f is a fracture permeability, k_c is a volume cell permeability, and A_c volume cell cross section area. We used cubic law (Adler at el., 2013) to calculate fracture permeability, k_f, from fracture aperture, b_f:

$$k_f = b_f^2/12. \quad (3)$$

We perform described above rescaling calculations for porosity and permeability assignment for each volume cell in the continuum mesh. After rescaling, we end up with $3.28 \cdot 10^{-4}$ as a mean porosity value for volume cells that contain fracture, and $2.7 \cdot 10^{-13}$ m^2 is an effective permeability mean value for volume cells with fracture.

2.3 Simulation Experiment Setup

The physical Expt 1 network at the EGS Collab site most likely has complicated natural fractures geometry, heterogeneities in the rock fabric, natural fractures, spatial variations of in-situ stress, and other geologic features. To understand heat and tracer transport in fractured media we used three basic setups of varying complexity. Three different fracture setups include: 1) a single channel flow; 2) three discrete fracture network (3DFN), and 3) common discrete fracture network (CDFN). The CDFN setup represents our understanding of the natural fractures' locations and orientations at the Expt 1 site (Roggenthen and Doe, 2018, Schwering et al., 2018, Ulrich et al, 2018). All three setups are shown in Figure 4. In all three setups we assume that injection borehole is well-insulated and there is no heat exchange while liquid travels along the E1-I borehole. The liquid is injected into the stimulated fracture or channel at a point corresponding to the intersection of channel/stimulated fracture with E1-I borehole. In the single channel setup, we have highly permeable direct path in the stimulated fracture connecting E1-I and E1-P boreholes (Figure 4a, gray thin line, which connects injection and production wells). In this configuration the 100% of injected liquid gets collected at the E1-P. In the other two setups, we collect flow from three different locations: E1-P, E1-OB, and at the E1-PInt. The E1-P, E1-OB production wells corresponding to the intersection of the production borehole with the stimulated facture and the intersection of the E1-OB monitoring borehole with the stimulated fracture (Figure 4bc). The E1-PInt location corresponds to the intersection point of the production borehole with the fracture parallel to the stimulated fracture for the 3DFN setup (Figure 4b), and to the intersection point of the production borehole with the OT-P connector (a fracture passing through the E1-P borehole couple feet below the production point) for the CDFN case (Figure 4c).

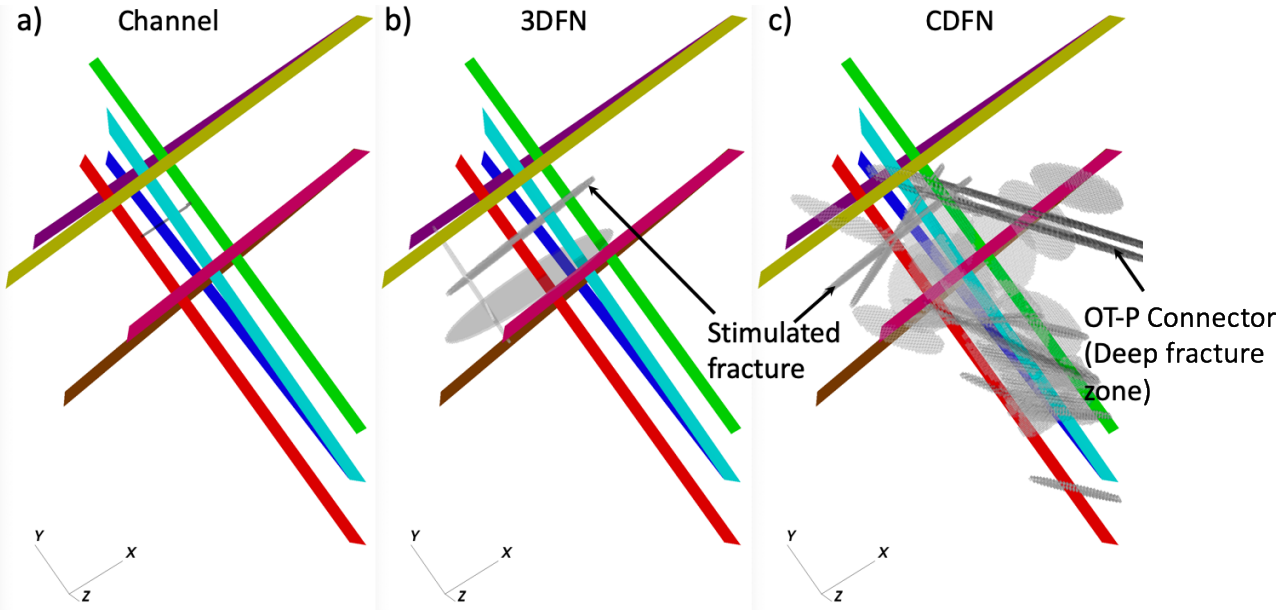

Figure 4: Discrete fracture network setup for three numerical experiments: (a) one channel, gray thin line, which connects injection and production wells; (b) three discrete fracture network (3DFN); and (c) common discrete fracture network (CDFN). Solid colored lines represent boreholes layout within the testbed. Injection [E1-I] borehole shown in red and production [E1-P] borehole shown in green, other six boreholes are the monitoring wells.

2.4 Flow-thermal-tracer modeling

PFLOTRAN is a multiphase flow and reactive multicomponent transport simulator that solves a system of generally nonlinear partial differential equations describing multiphase, multicomponent and multiscale reactive flow, reactive transport and geomechanics in porous media (Hammond et al., 2014; Lichtner et al., 2015). PFLOTRAN is an open-source object-oriented code that can be downloaded from https://www.pflotran.org. This code was originally developed as part of the Department of Energy SciDAC-2 groundwater program and as a result of multiple U.S. Department of Energy National Laboratories effort. It is built on top of PETSc (Portable, Extensible Toolkit for Scientific Computation) framework (Balay et al., 2017), and incorporates PETSc's parallel data structures, linear and non-linear solvers, and relies on domain decomposition for parallelism.

To better understand flow and transport mechanisms at the Expt 1 site, we simulate chilling and tracer experiments. PFLOTRAN uses mode notation to define corresponding physical process (Lichtner, 2001). We used fluid flow and heat transfer mode coupled with tracer transport mode to setup PFLOTRAN input file. Similar fluid flow and heat transfer setup was used by Mudunuru et al., (2017). Here,

we skip the description of the governing equations because all of them are well documented in PFLOTRAN User Manual by Lichtner (2001).

Over the simulated time period we know that higher flow rate of collected flow was measured at the E1-PInt. So, in 3DFN and CDFN setups we assign 50% of the flow rate at E1-PInt, and 25% at E1-P and E1-OB each. In all three setups the system is closed, so that we collect 100% of the injected liquid in total. Collecting 100% of the injected liquid is also important for the numerical convergence of the model. The values of the flow rates at each well for every setup are shown in Table 1. The rock properties used in all three simulations are shown in Table 2 and might not necessarily match actual parameters observed at the Expr 1 site.

We simulated the chilling experiment based on the hourly averaged data from the Expt 1 site. Here, we use only averaged temperature data from the injection point at E1-I to simulate chilling experiments. The temperature at the injection well was recorded every 10 sec. The total simulation time interval is equal to 3,500.00h. Here, we assume a fully saturated system for all three cases. We used homogeneous temperature of 30.2 ^{o}C and hydrostatic pressure distribution at the initial time step. The system is closed and flow occurs only within the defined fractures between injection and production wells. In addition, we set 1 ^{o}C temperature gradient between injection and production wells to illustrate how temperature gradient would affect simulated temperatures at the producing wells. Finally, the tracer experiment includes tracer injection before and after the first chilling test over 5 minutes time interval. The tracer was injected twice: at 1 hour and at 800 hours of the simulation time.

Table 1. Flow rates used for three setups.

Wells	**Channel** [L/min]	**3DFN** [L/min]	**CDFN** [L/min]
E1-I	0.4	0.4	0.4
E1-P	0.4	0.1	0.1
E1-PInt	0	0.2	0.2
E1-OB	0	0.1	0.1

Table 2. Rock matrix properties used in the model.

Physical properties	**Rock**
Tortuosity [-]	0.1
Density [kg/m^3]	2716
Specific heat [J/(K kg)]	820
Thermal conductivity [W·m^{-1}·K^{-1}]	5.0
Porosity [-]	0.003
Permeability [m^2]	10^{-20}
van Genuchten α	0.001
van Genuchten λ	0.75
Residual saturation [-]	0.1

3. RESULTS

3.1 Thermal simulation

Simulated temperatures for all three setups at the E1-P are shown in Figure 5. In all experiments, we used hourly averaged temperature time-series at the injection point (E1-I) colored in black. The overall temperature decrease after 3500h is equal to -2.8 ^{o}C for channel setup and -0.38 ^{o}C for CDFN and 3DFN setups, respectively. These results indicate that for CDFN and 3DFN cases the injected liquid flows equally in all directions of the circular fracture. Similarly, heat flow in these cases is distributed around the fracture and has a shape of sphere, with the coldest temperature at the injection point. In the channel setup, the heat is directed towards the production well, causing the production well respond faster to temperature changes at the injection well. The snapshots of simulated heat distribution from injected well to rock matrix is shown in Figure 6 for fractured media (3DFN and CDFN) and channeled flow. The final time snapshot shows directed heat flow along simulated channel from injection source to production locations (Figure 6b).

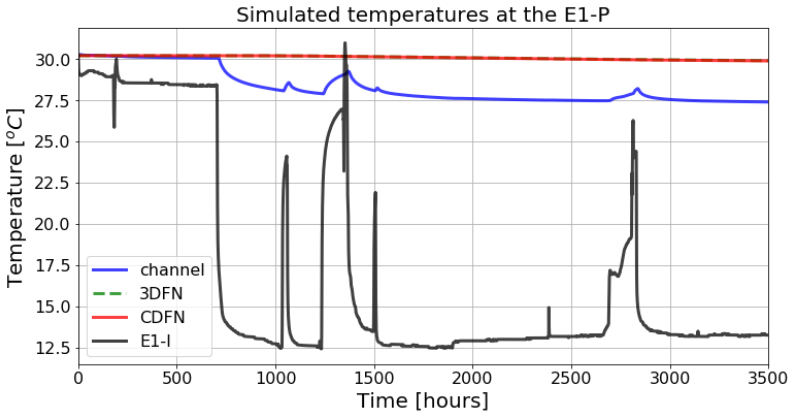

Figure 5: Simulated temperature time-series at E1-P for all three fracture setups. The black line shows the injected temperature profile at the injection well E1-I.

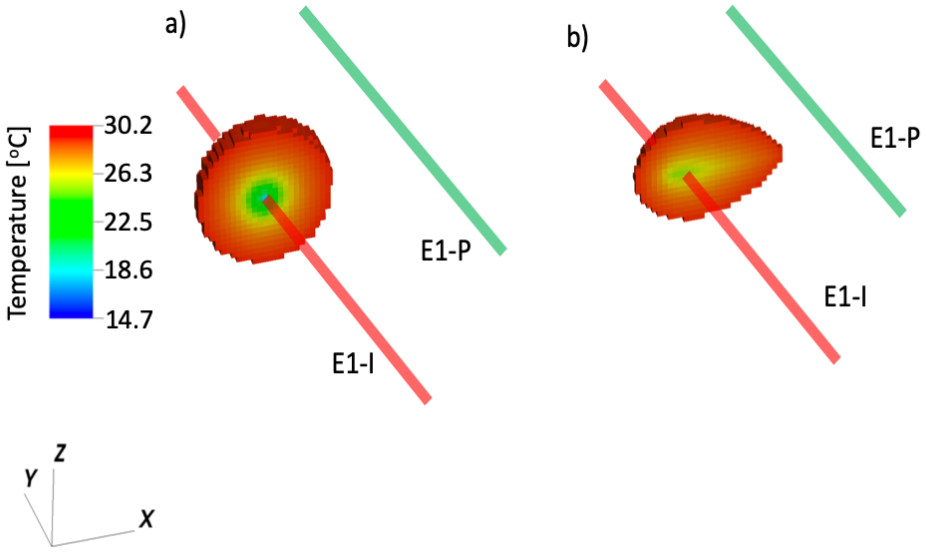

Figure 6: Temperature snapshot of simulated heat distribution for a) CDFN and 3DFN setups, and b) channeling flow. Here we threshold the temperature at 29 °C and then cross cut it in the middle to illustrate the coldest temperatures at the injection point.

Simulated temperature time-series at E1-Pint and E1-OB for 3DFN and CDFN setups are shown on Figure 7. As it was mentioned above, temperature at E1-I cools equally in all directions when directed channel flow is not considered (Figure 6a). The results for E1-PInt show slight temperature increase first 1000 hours for 3DFN setup (Figure 7a). The CDFN setup does not show that temperature increase, because CDFN has a direct connection with the stimulated fracture, while the 3DFN setup does not provide direct fracture connection with stimulated fracture. The temperatures at the E1-OB show gradual decrease over time with both 3DFN and CDFN setups, where temperature at 3DFN decreases slightly faster. No fractures on the flow path towards E1-OB for the 3DFN setup lead to slightly faster cooling in comparison to the CDFN setup (Figure 7b).

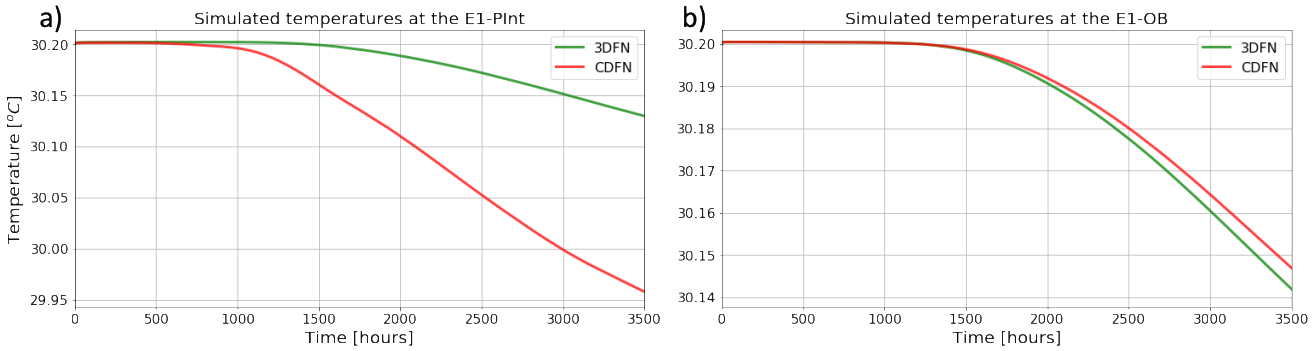

Figure 7: Simulated temperature time-series at (a) E1-Pint and (b) E1-OB for three fracture network (3DFN) and Common DFN setups respectively.

To illustrate the effect of the temperature gradient between injection and production wells, we use 3DFN and CDFN setups with applied 1 ºC temperature gradient between injection and production wells. The results indicate temperature increase over some period of time at all wells for both cases (see Figure 8). The highest temperature increase was obtained at the E1-Pint for 3DFN, the temperature increase lasted for 1500h indicating the effect of the temperature increase at E1-PInt can be greater when there is a temperature difference between wells (Figure 8a). The longer lasting temperature increase for the 3DFN setup at E1-PInt suggests that increasing the number of fractures (i.e. longer flow pathway) between E1-I and E1-PInt would lead to even longer time period for temperatures increase at E1-PInt. In contrast, CDFN case showed similar to E1-P temperature behavior over first 1000 hours (Figure 8b). Since there is a direct pathway linking E1-I and E1-P the temperature at the E1-P decreases faster than at E1-Pint point during chilling injection. Note, E1-PInt has twice higher flow rate production than other two production well, suggesting that high volume of storage water could be pushed out from other connected factures. After sufficient mixing of the injected fluid with the storage water, the temperature at E1-PInt started to decrease (Figure 8b). The temperature profile obtained at the E1-OB shows similar dynamics, which is expected, since E1-PInt and E1-OB are both located on the stimulated fracture.

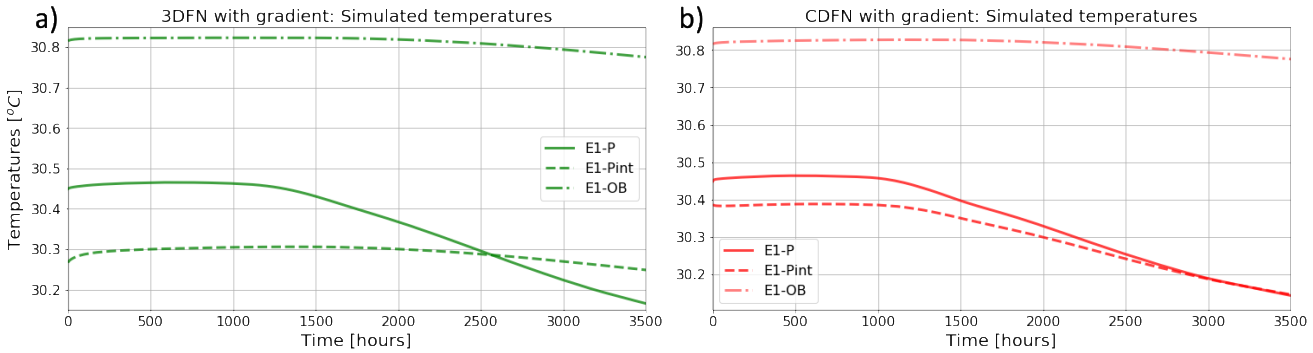

Figure 8: Simulated temperature time-series at all three wells for (a) 3DFN and (b) CDFN setups. In both cases, we set 1 ºC temperature gradient between injection and production wells.

3.2 Tracer simulations

Since tracer simulation for the channel setup is straight forward, we show tracer simulation for 3DFN and CDFN setups only (Figure 9). The tracer simulations before and after the chilling test showed slight reduction in tracer concentration after chilling test (e.g. Figure 9ac). The reduction in tracer concentration can be attributed to changes in liquid density after chilling test. The 3DFN setup showed later tracer arrival at the E1-PInt in comparison to the CDFN setup (e.g. Figure 9ab). The E1-OB well shows almost immediate tracer arrival for the 3CDFN setup and lags behind the E1-PInt for the CDFN setup. The results of the tracer experiment showed that if there is no direct connection between E1-I and E1-PInt, then the tracer arrival time at E1-PInt lags behind the E1-OB, located at the stimulated fracture.

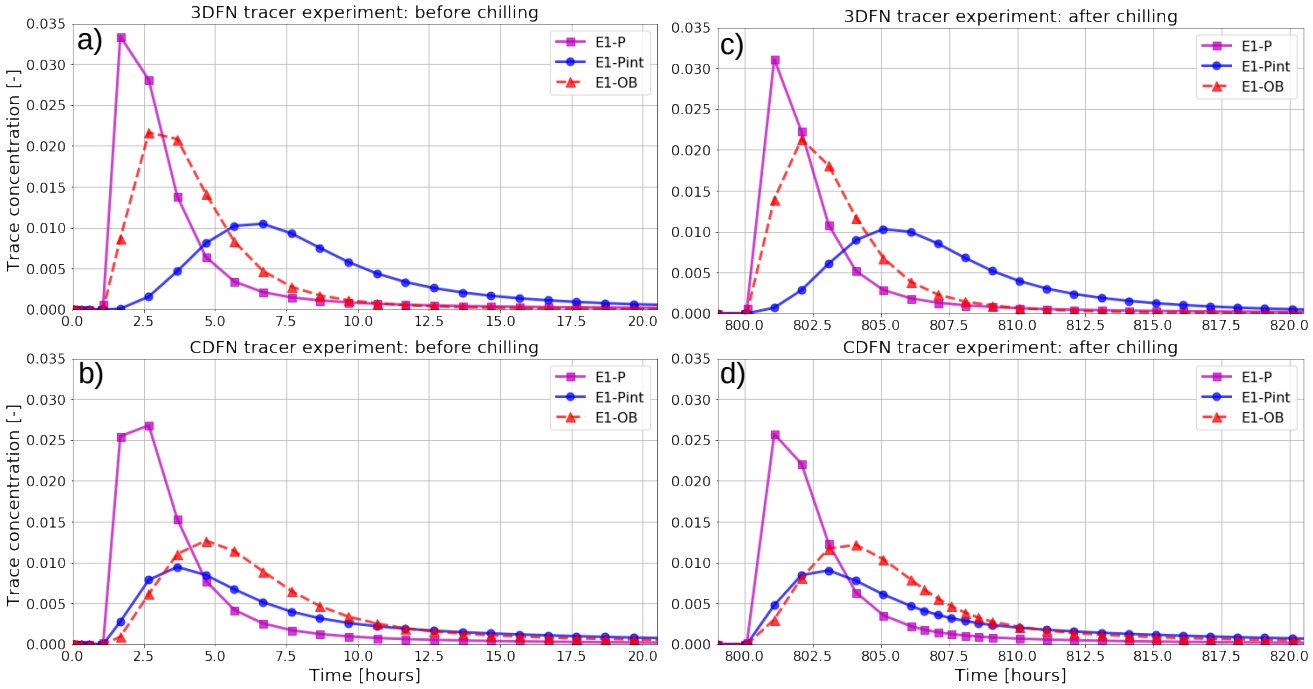

Figure 9: Tracer transport simulations for (a, c) three fracture network (3DFN) and for (b, d) CDFN setups before and after chilling test, respectively.

4. CONCLUSION

In the current study, we presented dfnWorks-PFLOTRAN modeling framework developed to simulate heat flow and tracer transport in three-dimensional fractured media. We used three different fracture geometry setups: channel setup - direct path between the injection and the production wells; 3DFN – discrete fracture network that consists of three connected fractures; and Common DFN, discrete fracture network similar to those observed during core inspections from the drilled boreholes (Roggenthen and Doe, 2018, Schwering et al., 2018). In all considered cases the distance between injection (E1-I) and production wells (E1-P) was the same, 10 meters.

We numerically showed, that the channel setup was the most sensitive to temperature changes at the injection well, and the overall temperature decrease at the production well, E1-P, obtained during chilling test, was -2.8 ^{o}C. 3DFN and CDFN setups showed more gradual temperature decrease at the E1-P than channeling, with the overall temperature decrease -0.38 ^{o}C. Numerical experiments simulated in this study indicate gradual cooling when applied to the stimulated fracture. In addition, negative temperature gradient between injection and production wells might lead to temperature increase at the producing locations.

Modeling results with 1 ^{o}C temperature gradient between E1-I and E1-P indicated temperature increase over some period of time at all considered producing locations. The 3DFN setup showed that temperature increase time interval could be extended when the path between injection and collection well (E1-PInt) increases (see Figure 8a). Similarly, tracer transport simulations showed later tracer arrival at E1-PInt for 3DFN setup in comparison to CDFN setup.

The CDFN setup used in this study represents a realization of our current understanding of the core fracture geometry observed in Expt 1 site. The actual natural fracture geometry at the site is more complicated than the fracture network that was detected at the borehole's cores. Therefore, further work might include adding stochastically distributed fractures into the CDFN. Solving stochastic fracture network system is computationally expensive task and would require statistically significant number of cases in order to draw meaningful conclusions.

ACKOWLEDGMENTS

This material was based upon work supported by the U.S. Department of Energy, Office of Energy Efficiency and Renewable Energy (EERE), Office of Technology Development, Geothermal Technologies Office, under Contract No. 89233218CNA000001 to Los Alamos National Laboratory (LANL). LANL is operated by Triad National Security, LLC, for the National Nuclear Security Administration (NNSA) of U.S. DOE. The United States Government retains, and the publisher, by accepting the article for publication, acknowledges that the United States Government retains a non-exclusive, paid-up, irrevocable, world-wide license to publish or reproduce the published form of this manuscript, or allow others to do so, for United States Government purposes. The research supporting this work took place in whole or in part at the Sanford Underground Research Facility in Lead, South Dakota. The assistance of the Sanford Underground

Research Facility and its personnel in providing physical access and general logistical and technical support is acknowledged. The hydrostructural model was created using FracMan software (Golder Associates, Inc.).

REFERENCES

Adler, P. M., J.-F. Thovert, and Mourzenko, V. V.: Fractured porous media. Oxford University Press, (2013).

Balay, S., S. Abhyankar, M. Adams, J. Brown, P. R. Brune, K. Buschelman, V. Eijkhout, W. Gropp, D. Kaushik, M. G. Knepley, and Others: PETSc user's manual revision 3.8. *Technical report*, Argonne National Laboratory, ANL, (2017).

Dershowitz, W. S.: Rock joint systems. Ph. D. thesis, Massachusetts Institute of Technology, (1984).

Dershowitz, W.: FracMan version 7.4-Interactive discrete feature data analysis, geometric modeling, and exploration simulation: *User documentation*, http://fracman.golder.com/, (2014).

Dobson, P, Asanuma, H., Huenges, E., Poletto, F., Reinsch, T., et al.: Supercritical Geothermal Systems - A Review of Past Studies and Ongoing Research Activities. *42nd Workshop on Geothermal Reservoir Engineering*, Stanford, CA, United States, (2017).

Hammond, G.E., and Lichtner, P.C.: Field-scale model for the natural attenuation of uranium at the Hanford 300 Area using high performance computing, *Water Resources Research*, **46**, W09527, doi:10.1029/2009WR008819, (2010), 1-31.

Hammond, G. E., Lichtner, P. C., and Mills, R. T.: Evaluating the performance of parallel subsurface simulators: An illustrative example with PFLOTRAN, *Water Resources Research*, **50**, (2014), 208– 228.

Hyman, J. D., S. Karra, N. Makedonska, C. W. Gable, S. L. Painter, and H. S. Viswanathan: dfnWorks: A discrete fracture network framework for modeling subsurface flow and transport, *Computational Geosciences*, **84**, (2015), 10–19.

Kneafsey, T.J., Dobson, P., Blankenship, D., Morris, J., Knox, H., Schwering, P., White, M., Doe, T., Roggenthen, W., Mattson, E., Podgorney, R., Johnson, T., Ajo-Franklin, J., Valladao, C., and the EGS Collab team: An overview of the EGS Collab project: Field validation of coupled process modeling of fracturing and fluid Flow at the Sanford Underground Research Facility, Lead, SD, PROCEEDINGS, *the 43rd Workshop on Geothermal Reservoir Engineering*, Stanford University, Stanford, California, SGP-TR-213, (2018).

Karra, S., Painter, S. L., Lichtner, P. C.: Three-phase numerical model for subsurface hydrology in permafrost-affected regions (PFLOTRAN-ICE v1. 0), *The Cryosphere*, **8** (5), (2014), 1935-1950.

Karra, S., Makedonska, N., Viswanathan, H. S., Painter, S. L., and Hyman, J. D.: Effect of advective flow in fractures and matrix diffusion on natural gas production, *Water Resources Research*, **51**, (2015), 8646–8657.

Los Alamos Grid Toolbox, LaGriT, Los Alamos National Laboratory, ⟨http:// lagrit.lanl.gov⟩, (2018).

Lichtner, P., G. Hammond, C. Lu, S. Karra, G. Bisht, B. Andre, R. Mills, J. Kumar: PFLOTRAN user manual: A massively parallel reactive flow and transport model for describing surface and subsurface processes, *Tech. Rep. Report No.: LA-UR-15-20403*, Los Alamos National Laboratory, (2015).

Lichtner, P.C.: PFLOTRAN User Manual. *Technical Report LA-UR-01–2349*, LANL, (2001).

Lichtner, P., S. Karra,: Modeling multiscale-multiphase-multicomponent reactive flows in porous media: Application to CO2 sequestration and enhanced geothermal energy using PFLOTRAN, in: Al-Khoury, R., Bundschuh, J. (eds.) *Computational Models for CO2 Geo-sequestration & Compressed Air Energy Storage* (http://www.crcnetbase.com/doi/pdfplus/10), CRC Press, (2014), 81-136.

Lu, C., Lichtner, P. C.: High resolution numerical investigation on the effect of convective instability on long term CO2 storage in saline aquifers, in: *Journal of Physics: Conference Series*, **78**, IOP Publishing, (2007), 012042.

Makedonska, N., Painter, S.L., Bui, Q.M. et al.: Particle tracking approach for transport in three-dimensional discrete fracture networks *Computational Geosciences*, **19**, (2015), 1123.

Makedonska, N., Jafarov, E., Doe, T., Schwering, P.C., Neupane, G., and EGS Collab Team: Simulation of injected flow pathways in geothermal fractured reservoir using discrete fracture network model, *In 45th Workshop on Geothermal Reservoir Engineering*, Stanford, CA, (2020).

Middleton, R. S., Carey, J. W., Currier, R. P., Hyman, J. D., Kang, Q., Karra, S., Jiménez-Martínez, J., Porter, M. L., & Viswanathan, H. S.: Shale gas and non-aqueous fracturing fluids: Opportunities and challenges for supercritical CO2. *Applied Energy*, **147**, (2015), 500–509.

Mudunuru, M. K., Karra, S., Harp, D. R., Guthrie, G. D. & Viswanathan, H. S.: Regression-based reduced-order models to predict transient thermal output for enhanced geothermal systems. *Geothermics*, **70**, (2017), 192–205.

Neupane, G. H., Podgorney, R. K., Huang, H., Mattson, E. D., Kneafsey, T. J., Dobson, P. F., Schoenball, M., Ajo-Franklin, J. B., Ulrich, C., Schwering, P. C., Knox, H. A., Johnson, T. C., White, M. D., Roggenthen, W., Doe, T. W., Blankenship, D. A., Vermeul, V. R., and Strickland, C. E.: EGS Collab Earth Modeling: Integrated 3D Model of the Testbed. *GRC Transactions*, (2019).

Roggenthen, W.M., and T.W.: Doe Natural Fractures and Their Relationship to the EGS Collab Project in the Underground of the Sanford Underground Research Facility (SURF), in *52nd U.S. Rock Mechanics/Geomechanics Symposium*, edited, p. 11, American Rock Mechanics Association, Seattle, Washington, doi:https://doi.org/, (2018).

Schwering, P.C., Blankenship, D., Podgorney, R.K., Neupane, G.H., Doe, T., Ulrich, C., Dobson, P.F., Kneafsey, T.J., Singh, A., Smith, M.M. and Roggenthen, W.: The First EGS Collab Testbed at the Sanford Underground Research Facility-Discrete Fracture Network Characterization. In *AGU Fall Meeting Abstracts*, (2018).

Ulrich, C., Dobson, P.F., Kneafsey, T.J., Roggenthen, W.M., Uzunlar, N., Doe, T.W., Neupane, G., Podgorney, R., Schwering, P., Frash, L. and Singh, A.: The distribution, orientation, and characteristics of natural fractures for Experiment 1 of the EGS Collab Project, Sanford Underground Research Facility. *In Proceedings, 52nd US Rock Mechanics/Geomechanics Symposium*, American Rock Mechanics Association, ARMA 18-1252, (2018).

U.S. Department of Energy, Energy Efficiency & Renewable Energy, Geothermal Technologies Office. 2016 Annual Report Geothermal Technologies Office, Retrieved, https://energy.gov/sites/prod/files/2017/03/f34/GTO20201620Annual20Report_0.pdf; (2017).

White, M., P. Fu, H. Huang, A. Ghassemi, and E.C. Team: The Role of Numerical Simulation in the Design of Stimulation and Circulation Experiments for the EGS Collab Project in *GRC Transactions*, **41**, edited, (2017).

White, M., T. Johnson, T. Kneafsey, D. Blankenship, P. Fu, H. Wu, A. Ghassemi, J. Lu, H. Huang, G. Neupane, C. Oldenburg, C. Doughty, B. Johnston, P. Winterfeld, R. Pollyea, R. Jayne, A. Hawkins, Y. Zhang, and EGS Collab Team,: The Necessity for Iteration in the Application of Numerical Simulation to EGS: Examples from the EGS Collab Test Bed 1, in *44th Workshop on Geothermal Reservoir Engineering*, edited, Stanford University, Stanford, California, (2019).